Elsevier Editorial System(tm) for Energy Conversion and Management
Manuscript Draft

Manuscript Number: ECM-D-14-03050R1

Title: A novel solar multifunctional PV/T/D system for green building roofs

Article Type: Original research paper

Section/Category: 1. Energy Conservation and Efficient Utilization

Keywords: solid CPC； solar PV/T/D system； high efficiency utilization； green building roof；avoid overheating and dazzling； visual comfort for building occupants.

Corresponding Author: Ms. chaoqing feng, PH.D

Corresponding Author's Institution: Beijing Institute of Technology

First Author: chaoqing feng , PH.D

Order of Authors: chaoqing feng , PH.D; hongfei zheng, PH.D; rui wang, PH.D; xu yu, PH.D; yuehong su, PH.D

Abstract: A novel transparent roof which is made of solid CPC (Compound Parabolic Concentrator) PV/T/D (Photovoltaic/Thermal/Day lighting) system is presented. It combines the solar PV/T/D system with green building design. The PV/T/D system can achieve excellent light control at noon and adjust the thermal environment in the building, such that high efficiency utilization of solar energy could be achieved in modern architecture. This kind of roof can increase the visual comfort for building occupants; it can also avoid the building interior from overheating and dazzling at noon which is caused by direct sunlight through transparent roof. Optical simulation software is used to track the light path in different incidence angles. CFD (Computational Fluid Dynamics) simulation and steady state experiment have been taken to investigate the thermal characteristic of PV/T/D device. Finally, the PV/T/D experimental system was built; and the PV efficiency, light transmittance and air heating power of the system are tested under real sky conditions.

A novel solar multifunctional PV/T/D system for green building roofs

Chaoqing Feng[a,b], Hongfei Zheng[a, c], Rui Wang [a], Xu Yu[c], Yuehong Su [c]
[a]School of Mechanical Engineering, Beijing Institute of Technology, Beijing 100081, China
[b]College of Energy and Power Engineering, Inner Mongolia University of Technology, Hohhot 010051, China
[c]Institute of Sustainable Energy Technology, Department of Architecture and Built Environment, University of Nottingham, Nottingham NG7 2RD, UK

Abstract: A novel transparent roof which is made of solid CPC (Compound Parabolic Concentrator) PV/T/D (Photovoltaic/Thermal/Day lighting) system is presented. It combines the solar PV/T/D system with green building design. The PV/T/D system can achieve excellent light control at noon and adjust the thermal environment in the building, such that high efficiency utilization of solar energy could be achieved in modern architecture. This kind of roof can increase the visual comfort for building occupants; it can also avoid the building interior from overheating and dazzling at noon which is caused by direct sunlight through transparent roof. Optical simulation software is used to track the light path in different incidence angles. CFD (Computational Fluid Dynamics) simulation and steady state experiment have been taken to investigate the thermal characteristic of PV/T/D device. Finally, the PV/T/D experimental system was built; and the PV efficiency, light transmittance and air heating power of the system are tested under real sky conditions.

Keywords: solid CPC, solar PV/T/D system, high efficiency utilization, green building roof, avoid overheating and dazzling, visual comfort for building occupants.

0 Introductions

Research on PV/T/D (Photovoltaic/Thermal/Day lighting) system is a promising topic in solar energy applications, and many studies have been done on conventional solar concentrators. Kern [1] proposed the basic idea of PV/T (Photovoltaic/Thermal) utilization of solar energy in 1978, the method was that arranging the flow path at the back of PV cell, the thermal energy can be taken away by the flowing fluid and the collected energy could be used for forward thermal application. This method can not only cool the PV cell and increase the photoelectric efficiency, but also can fulfill the comprehensive utilization of solar energy[2-4]. The solar energy comprehensive use ratio can reach 60%-80% for PV/T system[5-7], Li M [8] , Tan L [9] and Ibrahim A[10] also tested the performance of PV/T system and taken some optimization design.

Combining the PV/T system with building is the developing tendency of green building in the future; it can increase the usage ratio of solar energy. When the CPV/T (Concentrate Photovoltaic/Thermal) technology was used in building, a higher concentrate ratio is expected in order to generate higher temperature for thermal energy. The high temperature heat source will expand its application field, such as solar heater, solar air-condition and solar dehumidification. It will increase the contribution of solar energy in the field of building energy conservation.

High efficiency solar concentrator has its shortcuts such as it requires high-cost accurate optical material, and the tracking system has many complicated moving parts, so it is difficult to combine it with building. In addition, the performance of normal PV cell cannot improve obviously[11]. On the contrast， the CPC (Compound Parabolic Concentrator) with lower concentration ratio is more feasible to combine with the building. Garg [12] and Brogren[13] reached the CPC-PV/T system with the concentrate ratio of 3 and 4, studies showed that the thermal and electric output of a PV/T system increases with increasing collector length, air mass flow rate and cell density, and decreases with enlarged in duct depth. Adsten M et al [14] evaluated the CPC collector for roof or wall application, Finally, a concentrating solar collector for wall mounting was evaluated with an estimated annual output of 194 MJ/m^2 at operating temperature of 75℃. Li G Q[15,16] and Pei G[17] taken some research about the efficiency of CPC-PV/T with different concentrate ratio, the thermal efficiency of CPC-type solar water heater system can be above 49.0% (attaining 95℃ water temperature). Recently, Li G [18] presents a novel static incorporated compound parabolic concentrator with photovoltaic/thermal system, the average value of optical efficiency within the half acceptance angle of 35° can achieve 83.0%.

Modern architecture structure design pays more attention on novel lighting and energy conservation, conventional CPC PV/T system will prevent the light into the building when it is used for the solar energy, this defect restricts the application field of the device. If the CPC PV/T system was made by transparent material, it will expand the application field and integrate with building easily. This transparent CPC PV/T system using in building can increase the visual comfort for building occupants. In the summer at noon, the sun light would transmit through the roof directly, transparent roof would cause overheating and dazzling in the building. In order to solve this problem, a novel transparent roof which is made of solid CPC PV/T/D system is presented. It integrates the solar energy PV/T/D system with building design. The PV/T/D system can control lights well at summer noon and adjust the thermal environment in the building; as a result, high efficiency utilization of solar energy is achieved in modern architecture.

1 Structure and working principle of PV/T/D system

The structure of a novel PV/T/D system is shown in Fig.1. It is consist of upper cover, lower cover and side plate, all of them are made by PMMA (Polymethyl methacrylate). The upper cover is composed by solid CPC. The PV cell was pasted on the undersurface of solid CPC. The light transmittance varies in accordance to the changing light incidence angles. The thickness of lower cover of PV/T/D device is 3mm, and there are 900 holes in this plate. The length and width of PV/T/D device are all 300mm, other sizes are marked in Fig.1, and unit is mm.

Fig.1 The working principle of the PV/T/D device

The working principle of a novel PV/T/D system is expressed briefly: sun light penetrates into the system from upper cover plate, light will be concentrated to the PV cell when the incidence angle is small; when the incidence angle is large, the light will escapes from the lateral wall of a solid CPC and provides daylighting to the building. The detailed optical principle of solid CPC was expressed by Yu Xu[19]. The PV cell could generates electrical energy as well as sufficient thermal energy, those thermal energy could heat the air between the upper and bottom plate, so the temperature of air is raised up. When the suction pump is working, the air would flow through the PV/T/D device and take away the warmed air for forward thermal application. This method can obtain additional thermal energy and fulfill the combination of PV and thermal energy, which raises the comprehensive utilization ratio of solar energy.

In the current study, the geometrical concentration ratio of solid CPC is 4, the right and left parabola equation of CPC is expressed by formula 1 and 2.

$$0.968y+0.2504x+75.1=\frac{\left(0.2504y-0.968x+72.6\right)^{2}}{375} \qquad (1)$$

$$0.968y-0.2504x+75.1=\frac{\left(0.968x+0.2504y+72.6\right)^{2}}{375} \qquad (2)$$

where *x* and *y* are coordinate in the Descartes, unit is m.

When the light irradiates the solid CPC in different incidence angles, it will be reflected and refracted by the different surface of solid CPC, the light path is shown in Fig.2.

Fig.2 Entity CPC optical path diagram

Fig. 2 illustrates two representative light paths within a solid CPC. One is effective electricity generating light, like the ray 1; it will be concentrated on the PV cell which is pasted on the base of a solid CPC. The incidence angle of ray 1 is α, the ray 1 is refracted into the solid CPC through the upper surface and then fully reflected by the lateral wall, and finally it will reach the edge between lateral wall and base of solid CPC. At the incidence point *A*, when the incidence angle is smaller than α, the ray will be concentrated to the base of CPC. Another type of incidence light is effective lighting ray, like the ray 2. The incidence angle of ray 2 is β, which is larger than α, so the ray 2 will escape from the lower side of lateral wall of CPC. It will be used to light the building.

2 Optical simulation

In order to analyze the light path in the entity CPC cover of PV/T/D device, lights with different incidence angles are tracked by the optical simulation software Light Tools. Assuming the incident light is parallel light, the entity CPC material is PMMA and it has high transparency, its refraction index is 1.5. The simulation result of light path in the entity CPC with different incidence angle is shown in Fig.3.

Fig.3 Optical path diagram of different incidence angles

It can be known from Fig.3, when the incidence angle is 0°, a part of light reach the surface on cell directly, another part of light reach the CPC surface and concentrated on the cell surface. All light achieve to the lower surface of solid CPC and none of them penetrate the solid CPC cover. With the increase of incidence angle, light begin to penetrate the solid CPC cover gradually. The lager the incidence angle is, the higher the transmittance is. When the incidence angle is 20°, the transmittance is 25%; when the incidence angle is 40°, the transmittance can reach 77%; when the incidence angle is 60° or lager, all the light pass through the solid CPC and none of them can be received by PV cell. Analyzing the light path when the incidence angle is 0°, it can be discovered that not all the lights can reach the PV cell, some of them take place the full reflection in the lower surface of solid CPC and cannot received by cell. In order to avoid this phenomenon, the anti-reflection coating was used between the lower surface of solid CPC and the PV cell in the experiment device.

To analyze the concentration effect of solid CPC, the Light Tools was used to simulate the light distribution in different incidence angles. The changing of transmittance, reflectivity and receiving rate of cell with different incidence angle are shown in Fig.4. There, transmittance is the proportion of that lights escape from the lateral wall of CPC accounts for total incident lights. Reflectivity is the proportion of that lights escape from the upper surface of CPC (because of some lights take place the full reflection in the lower surface of CPC) accounts for total incident lights. Receiving rate of cell is the proportion of that lights received by cell accounts for total incident lights.

Fig.4 Lights distribution of different incidence angles

It can be known from Fig.4 that the transmittance rises with the increasing of the incidence angle; while the reflectivity and receiving rate of cell are decreasing. When the incidence angle is small, a lot of lights were full reflected by the lower surface of solid CPC, there are about 50% of light full reflected with the 0° incidence angle. When the incidence angle is larger than 20°, the reflectivity decrease obviously, the reflectivity tends to become 0 when the incidence angle is larger than 30°. With the increase of the incidence angle, receiving rate of cell is decreasing and their relationship is near the linear. The change of the transmittance curve presents a trend which is rapid before becoming slow. The turning point of transmittance curve appears at the 30° incidence angle. At this incidence angle, the transmittance can reach 70%.

3 Thermal characteristic analysis of PV/T/D system

3.1 Thermal characteristic simulation

Firstly, in order to get the air heating efficiency of PV/T/D system in different air flow rates and different heating power, the CFD (Computational Fluid Dynamics) software has been used to simulate the thermal characteristic. The heat loss condition can be obtained at the same time. Simulation field of CFD model contain a part outer space of PV/T/D system, in this case, the air flow condition before inlet can be analyzed; the heat exchange between the wall of PV/T/D device and environment can be obtained.

In order to simplify the simulation model, the following are the assumptions made in the physical model.

1、the air flow is uncompressible and laminar in device；

2、heat generation only occurs in the PV cell;

3、The air flow rate is zero in environment, nature convection is the only way of heat-exchange on the exterior surface of device.

4、the properties of material are isotropic;

5、The working temperature is not very high and the difference in temperature is small, so the heat radiation is ignored in the simulation model.

The boundary condition of CFD simulation was set as follow：

a. Air inlet: inlet vent, temperature is 290K;

b. Air outlet: pressure outlet, the pressure is 2000 Pa;

c. The boundary condition of solar cell: wall, heat flux, assuming that the solar irradiance is 1000 w/m^2, the geometrical concentration ratios is 4, if the heating efficiency was 80%, so the heat flux can be calculated and was 3200w/m^2.

d. Solid CPC was defined as solid and its material was PMMA. The density is 1200kg/m^3, specific heat capacity is 1500 KJ/kg·K, heat transfer rate is 0.2W/m·K. The common boundary between solid and air was defined as wall, the boundary type was coupled.

e. the number of grids was 650,000.

f. Convergence criteria: Residuals of energy equation is 10^{-6}, others are 10^{-4}.

3.1.1 Temperature distribution

When the environment temperature is 290K, outlet static pressure is 2000Pa, the flow and heat transfer in calculate unit was shown in the fig.5, the same as the temperature distribution of lower surface, upper surface and cell surface.

Fig.5 Temperature distribution

It can be known from the temperature distribution of Fig.5 that when the distance from outlet is farther; the temperature in the lower surface and cell surface is higher. The reason is that the heat exchange of lower surface and cell surface mainly depend on force air flow of pump, air flow speed is higher on the outlet side, so the heat transfer rate is lager and the temperature is lower in this side. On the upper surface, the temperature distribution tendency is opposite with the lower surface, near the outlet the temperature of upper surface is higher than the other side, but the temperature different is only about 2℃. Given that the heat exchange of upper surface mainly depend on nature convection and it should have same convective heat transfer coefficient for the entire surface, the temperature difference of upper surface could be explained by the air flow in within the PV/T/D device, it could absorb the thermal energy from PV cell and bring it to the outlet, where the temperature is relatively higher, as a result, the warmed air heats the upper cover plate and causes the upper cover plate temperature near the outlet being higher than the another side . Additionally, it could also be observed from Figure 5b that temperature can reach 350K in the cell surface away from outlet. If the common PV cell is working in this temperature, it will largely reduce the electric generating efficiency.

3.1.2 Air heating efficiency

When the heat flux of cell surface is 3200 w/m^2, the total heating power of the device is 72W, the air heating efficiency and thermal characteristic of PV/T/D system can be obtained by simulation. Under the different air flow speeds, the air heat utilization efficiency and losses of the device are shown in table 1.

Table 1 The heat utilization efficiency and losses under different air flow speeds of the device

It can be known from Table 1 that under the same heating power, air heating efficiency increases with air flow rate increase. It is because that the growing air flow rate will increase the heat exchange rate between air and hot solar cell, it will lead to the reduced PV/T/D device temperature, as the heat exchange rate would be lower under lower temperature, the heat loss of the whole device would therefore be reduced. From the simulation results it can also be known that the heat loss on the lower surface is 1.5 times more than the upper surface, the heat loss on the lateral surface of device is very small.

3.2 Steady state experiment

Because the solar irradiance changes with the time, it cannot obtain the thermal characteristic of PV/T/D system in constant power. So the steady state experiment was taken in the room. The indoor experiment system is shown in Fig.6.

Fig.6 the photo of the indoor experimental system

Fig.6 is the photo of the indoor experimental system. The system consists of PV/T concentrator, ventilator, air pump, thermometer and anemometer.

The thermo-signal of the device was given by the K type thermocouples and the temperature value was read from a multiplex thermo-meter. 15 thermocouples were arranged as in Fig.7. The wind velocity was measured by a KA22 thermo-ball type wind-meter whose relative error is ±2%.

Fig.7 The arrange diagram of the thermo-couples in the device.

The experiment was completed indoor in which the electricity heater was used to simulate the heat energy produced on the PV panels by sunlight through CPC concentration. On each undersurfaces of the CPC, the electricity heater piece was pasted to produce the heat to represent that of sunlight by CPC concentration. The resistant of the electricity heater piece is 3480Ω. Connected heater pieces in parallel, the total resistant turned to 232Ω. From this value, the electricity voltage can be calculated to be 144V when the heat power is 90W.

3.2.1 Temperature increase

In the experiment, the given power was put into system, analyzing the temperature distribution inside the device point by point under a certain wind speed. Apparently, both temperature distribution in the system and air-heating state would change when input power is different. Fig.8 shows that the temperature curve of 16 measurement points (there, thermocouple 16 shows the environment temperature) of the system from the beginning to temperature reached stabilization when given power was 90W (the area of device's upper surface is 0.09 m^2, it corresponds to be put under solar irradiance about 1000W/m^2). At this time, 900 holes were distributed on ventilation gate of the device's backplane whose size was 30cm×30cm, and the diameter of each hole was 3mm. In this circumstance, the wind mass flow rate passing through the system was 21.9 kg/h.

Fig. 8 The variation of the temperature in different measuring points with the operation time

According to the Fig.8, even though the thermal inertia was a little low, it will take about 2000 seconds to make the device to reach the basic equilibrium. Concerning the device was in a cooling state, if the device was in a warming state, it would reach the basic equilibrium within a much shorter time. We can also find that, in the device, the temperature was distributed in an uneven way, which was increased overall from the ventilation gate to all directions. However, on the edge of the device, the temperature was decreased due to heat loss. T_1 was the highest temperature, reaching 46.2℃; T2 was the lowest temperature, which is 34.7℃. The average temperature from measuring points inside the device was 41.3℃, closing to T_8 and T_{13}. However, the average temperature of the device's surface was 25.9℃, closed to T_4. Thus, temperature difference of the air passing in and out was around 10℃. It can be explained that the temperature state inside the device can be changed by improving the thermal conductivity (like adding insulation layer to increase the average temperature inside the device and vent air's temperature) or adjusting holes' density and distribution to change the air-flowing situation in the device.

According to the condition of steady state experiment, the CFD simulation boundary conditions were set follow the experiment condition. Getting the temperature of test points from simulation results and comparing them with experiment results, the temperature and error are shown in Table 2.

Table2 the temperature comparing between simulation result and test result

From the experiment result in Table 2, it can be known that the distance with outlet is further; the temperature in the cell surface is higher. On the upper surface, the temperature of upper surface near the outlet is higher than another side, but the temperature difference is very little. The experiment results of temperature distribution were in good agreement with simulation results. From the table 2, it can be seen that, on the cell surface, the test point temperature of experiment result is lower than simulation result. This result may be because the radiation is ignored in the simulation model, so the simulation heat exchange rate of cell surface is lower than the real situation and the simulation temperature on the cell surface is higher. On the upper surface, the test point temperature of experiment result is higher than simulation result. Because the radiation is ignored in the simulation model, heats receive of upper cover in simulation is lower than the real situation, so the simulation result of temperature on upper surface is lower than the experiment result.

3.2.2 Experiments at different heating power

In order to understand the device's heat dissipation and air heat receiving condition accurately, the experimental system heat receiving and heat loss are calculated. In the case of different heating power, the changes of temperature difference between import and export are shown in Fig.9. Air inlet and outlet temperature difference reflects the heat receiving efficiency of air. As can be seen from the Fig.9, the bigger the heating power is, the greater the temperature difference between the air inlet and outlet become, and basically reflects the actual situation.

Fig.9 Variation of the Temperature difference between output and input and efficiency under steady state condition with the air heating power

As can be seen from Fig.9, with the increasing of heat power, the inlet and outlets' wind temperature of steady-state is rising, the useful power increases; meanwhile, the heat loss is rising. So the air heating efficiency of the device is decreasing with the increase of heating power, and it is resulted from the device's high inner temperature, causing too much radiation heat exchange to surroundings so that the heat loss is enhanced when increasing the heating power.

3.2.3 Experiments at different air flow rates

Changing the ventilation rate and remaining other conditions unchanged, the distribution of measuring points' temperature could be obtained with the same heating power under different air flow rates. Still assuming that solar irradiance is about 1000W/m^2, and heating power is selected as 90W.

Firstly, comparing the air heating efficiency of simulation result and experiment result in different air flow rates, the result is shown in Fig.10.

Fig.10 the air heating efficiency comparing between simulation result and experiment result

It can be observed from Fig.10 that the air heating efficiency increase with the air flow rate increase, the change of the air heating efficiency curve presents a trend which is rapid before becoming slow. The tendency of experimental and simulation results match well. The differences between experimental and simulation results are due to the reason that ignoring the heat radiation of device in simulation model which may lead to the increasing of air heating efficiency. The differences decrease with the air flow rate increase. It may be because the high air flow rate will decrease the average temperature of the PV/T/D device and decrease the temperature difference with environment, so the heat radiation in experiment becomes small. The experiment curve is closed to the simulation curve when the air flow rate is large.

4 Experiment under the real sky

Outdoor experiment was undertaken under real sky conditions. The system was arranged on the sunlight directly in which the major target is to investigate the temperature distribution of the PV/T/D system, the efficiency of PV cell, light transmittance and the air temperature increasing when the sunlight is in different incident angles.

The experiment system was built as the Fig.11, it mainly consist of an integral box (using the integrating sphere principle), PV/T/D system, K type thermocouples, temperature collect recorder, KA22 type wind speed meter, a light meter, a voltmeter, an ammeter, air pump, and so forth. The transmittance measurement was based on use of a photometric integrating box. The photometric integrating box is a cubic box with its internal surface painted matt white so that light can be diffusely reflected to the internal sensor. On the cover of the box, there is PV/T/D system and it admits the light into the box. An internal illuminance sensor is attached to the panel and points downward; the reason for pointing downwards is that it can avoid direct light and measure the reflected light only. Meanwhile another external sensor is placed upward near the PV/T/D system to measure the outside illuminance, which stands for the amount of light penetrating through the PV/T/D system. A concept of transmittance can be defined, which is expressed by Equation 3.

$$\text{Transmittance} = \frac{Lx_2}{Lx_1} \times 100\% \qquad (3)$$

where Lx_1 and Lx_2 are the external and internal illuminance at measuring point.

The PV cell used in experiment is the normal thin film cell, the photoelectricity efficiency is about 8%. The outdoor experiments were conducted in Beijing, China (39° 51′ 45″ N，116° 18′ 49″ E). Test date is 2013-11-04, sunny.

Test method: 1) Put the test device on horizontal ground and make sure that the front edge of the cover is vertical in the south direction; 2) Raise the back of the cover and make sure that the angle between the normal of the cover and ground is the biggest solar elevation angle (33.8°) on the test day, and ensure that the incidence angle is 0° at noon. Fix the devices and the test is beginning without tracked system

Environment temperature, solar irradiance and integral box illumination is shown in fig.12, PV efficiency, transmittance and air heating power of the system is shown in fig.13. The PV efficiency η is calculated by output electric power and input total solar energy, it is shown in Equation 4. Air heating power is evaluated by Equation 5.

$$\eta = \frac{V \times I}{S \times R} \times 100\% \tag{4}$$

$$P_{heating} = C_p m (T_{outlet} - T_{i}) \tag{5}$$

where V is voltage across the load, V; I is current, A; S is area of device, m^2; R is solar irradiation, w/m^2; P is air heating power, W; C_p is specific heat capacity, J/g.K; m is mass flow rate of air, g/s; T is temperature, K;

Fig.11 Experiment system

Fig.12 Environment temperature, solar irradiance and integral box illumination

From Fig.12, the greatest solar irradiance appears at about 12:00; the changing trend of the integral box illumination in one day is hump-shaped; and that peak values appear at

9:00 AM and 14:30 PM, respectively. When the irradiance is strongest, at noon, the illumination in the box is low. The reason is that the incidence angle is small at noon, so most incident light was received by PV cell and it reduced the transmittance. After 14:30 PM, the illumination in the box decrease with the solar irradiance decrease.

Fig.13 PV efficiency, transmittance and air heating power of the system

From Fig.13, it can be seen that the photoelectricity and air heating efficiency is the highest at noon. The solar energy utilization efficiency is best at noon. Experimental results show that the lowest transmittance is only 31%, and appears when there is strong sunshine at noon; while in the morning and afternoon, the transmittance of PV/T/D system can reach 60%. When the transmittance is lower (10:00-14:00), PV efficiency and air heating power are higher. The biggest efficiency of PV occurs at noon and the value is higher than 7%. Furthermore, the maximum air heating power is 55W, also occurs at noon. During the test period in one day, the solar energy received by experiment device is 1833 kJ; thermal energy collected by flow air is 677kJ, electricity generated by PV cell is 97 kJ. Although the PV/T/D system does not have obvious influence on the light intensity entering a room in the morning and afternoon, while substantially reduces light intensity at noon, it can improve the status of uneven illumination in a room in one day. Meanwhile, PV/T/D system can generate electricity and hot air by surplus light.

Furthermore, based on the configuration of experiment device, the cost has been analyzed. PMMA plates and PV cells are the mainly cost of this device. The cost of this roof is about 210 dollar/m^2, in which the price of PMMA is about 110 dollar/m^2 and flexible solar cell price is about 100 dollar/m^2. Recently, the price of roof made by glass curtain wall is about 160~320 dollar/m^2. Comparing with the conventional glass roof, the cost of novel roof presented here is in the price range of the glass roof. So the novel roof is better than the conventional glass roof.

5 Conclusion

Combining the solar energy PV/T/D system with green building design, a novel transparent roof which is made by solid CPC PV/T/D system is presented. The novel building-integrated PV/T/D roofing design can achieve excellent light control at noon and improve the thermal environment in the building. Higher efficiency of solar energy utilization could be achieved in modern architecture with the new roofing technologies. If the users mainly concern about the interior temperature adjust during summer and winter, the roof should be placed in the way of that the axis of solid CPC is vertical with the east direction. In summer, solar elevation angle is large at noon and the novel roof can prevent sunlight into room; in the morning and afternoon, solar elevation angle is small and roof has high transmittance. In winter, solar elevation angle is small all the day, so the novel roofs can maintain high transmittance and let sunlight into the house.

Optical simulation software is used to track the light path in different incidence angles. With the increase of the incidence angle, receiving rate of cell is decreasing and their relationship is almost linear. The change of the transmittance curve presents a trend which is rapid before becoming slow. The turning point of transmittance curve appears at the 30°

incidence angle. At this incidence angle, the transmittance can reach 70%.

CFD simulation and steady state experiment have been done to investigate the thermal characteristic of PV/T/D device. The results showed that the air heating efficiency of the device is increasing with the increase of air flow rate and the decrease of heating power. Under real sky conditions, PV efficiency, transmittance and air heating power of the system are tested. The lowest transmittance is only 31%, and appears when there is strong sunshine at noon; while in the morning and afternoon, the transmittance of PV/T/D system can reach 60%. When the transmittance is lower (10:00-14:00), PV efficiency and air heating power are higher. The biggest efficiency of PV occurs at noon and the value is higher than 7%. Furthermore, the maximum air heating power is 55W, also occurs at noon. Although the PV/T/D system has no obvious influence on the light intensity entering a room in the morning and afternoon, while substantially reducing light intensity at noon, it can improve the status of uneven illumination in a room in one day. Meanwhile, PV/T/D system can generate electricity and hot air by surplus light.

Also, comparing with the conventional glass roof, the cost of novel roof is in the price range of the glass roof. So the novel roof is better than the conventional glass roof, it will has broad application prospects.

Acknowledgements

This work is supported by the National Natural Science Foundation of China (No.U1261119). The authors would also like to thank the national high technology "863" project of China（2013AA102407-2）.

References

[1] Kern Jr E C, Russell M C. Combined photovoltaic and thermal hybrid collector system [C]. Proceedings of the13th IEEE Photovoltaic Specialists, 1978, Washington DC, USA, 1153-1157.

[2] Bergene T, Lovvik M. Model calculations on a flat-plat solar heat collector with integrated solar cells[J]. Solar Energy, 1995, 55: 453-462.

[3] Rosell J I, Vallverdu X, Lechon M A, Ibanez M. Design and simulation of a low concentrating photovoltaic/thermal system [J]. Energy Conversion and Management, 2005, 46:3034-3046.

[4] Ji J, Han J, Chow T T, et al. Effect of flow channel dimensions on the performance of a box-frame photovoltaic/thermal collector[J]. Proceedings of the Institution of Mechanical Engineers, Part A: Journal of Power and Energy, 2006, 220(7):681-688.

[5] T T Chow, G Pei, K F Fong, et al. Energy and exergy analysis of photovoltaic-thermal collector with and without glass cover [J]. Applied Energy, 2009, 86(3):310-316.

[6] Naewngerndee R, Hattha E, Chumpolrat K, et al. Finite element method for computational fluid dynamics to design photovoltaic thermal (PV/T) system configuration [J]. Solar Energy Materials and Solar Cells. 2011, 95(1): 390-393

[7] Coventry J S, Lovegrove K. Development of an approach to compare the value of electrical and thermal output from a dometic PV/thermal system[J]. Solar Energy, 2003, 75(1):63-72.

[8] Li M, Li G L, Ji X, et al. The performance analysis of the trough concentrating solar photovoltaic/thermal system[J]. Energy Conversion and Management, 2011, 52:

2378-2383.

[9] Tan L, Ji X, Li M, et al. The experimental study of a two-stage photovoltaic thermal system based on solar trough concentration[J]. Energy Conversion and Management, 2014, 86: 410-417.

[10] Ibrahim A, Othman M Y, Ruslan M H, et al. Recent advances in flat plate photovoltaic/thermal (PV/T) solar collectors [J]. Renewable and Sustainable Energy Reviews. 2011,15 (1): 352-365.

[11] Wu Yuting , Zhu Hongye , Ren Jianxun, et al. Thermal and power characteristics of ordinary solar cells in concentrating solar collectors[J]. Journal of Tsinghua University, 2003, 43(8):1052-1055.

[12] Garg H P, Adhikari R S. Performance analysis of a hybrid photovoltaic/thermal (PV/T) collector with integrated CPC troughs [J]. International journal of energy research, 1999, 23(15): 1295-1304.

[13] Brogren M, Nostell P, Karlsson B. Optical efficiency of a PV-Thermal hybrid CPC module for high latitudes [J]. Solar Energy, 2001, 69: 173-185.

[14] Adsten M, Helgesson A, Karlsson B. Evaluation of CPC-collector designs for stand-alone, roof-or wall installation [J]. Solar energy, 2005, 79(6): 638-647.

[15] Li Guiqiang, Pei Gang, SuYuehong et al. Preliminary study based on building-integrated compound parabolic concentrators (CPC) PV/thermal technology[J]. Energy Procedia, 2012, 14: 343-350.

[16] Li Guiqiang, Su Yuehong, Pei Gang et al. Preliminary experimental comparison of the performance of a novel lens-walled compound parabolic concentrator (CPC) with the

conventional mirror and solid CPCs[J]. International Journal of Green Energy, 2013, 10(8): 848-859.

[17] Pei Gang, Li Guiqiang, Zhou Xi et al. Experimental study and exergetic analysis of a CPC-type solar water heater system using higher-temperature circulation in winter. Solar Energy, 2012, 86(5), 1280-1286.

[18] Li G, Pei G, Yang M, et al. Optical evaluation of a novel static incorporated compound parabolic concentrator with photovoltaic/thermal system and preliminary experiment[J]. Energy Conversion and Management, 2014, 85: 204-211.

[19] Yu X, Su Y H, Zheng H F, et al. A study on use of miniature dielectric compound parabolic concentrator (dCPC) for daylighting control application[J]. Building and Environment, 2014, 74: 75-85.

Captions

Figure captions:

Fig.1 The working principle of the PV/T/D device

Fig.2 Entity CPC optical path diagram

Fig.3 Optical path diagram of different incidence angles

Fig.4 Lights distribution of different incidence angles

Fig.5 Temperature distribution

Fig.6 the photo of the indoor experimental system

Fig.7 The arrange diagram of the thermo-couples in the device.

Fig. 8 The variation of the temperature in different measuring points with the operation time

Fig.9 Variation of the Temperature difference between output and input and efficiency under steady state condition with the air heating power

Fig.10 the air heating efficiency comparing between simulation result and experiment result

Fig.11 Experiment system

Fig.12 Environment temperature, solar irradiance and integral box illumination

Fig.13 PV efficiency, transmittance and air heating power of the system

Table captions:

Table 1 The heat utilization efficiency and losses under different air flow speeds of the device

Table 2 The temperature comparing between simulation result and test result

Table(s)

Table 1

Table 1 The heat utilization efficiency and losses under different air flow speeds of the device

Outlet air flow rate / kg/h	Air absorbs heat/W	Losses on upper surface/W	Losses on lower surface/W	Losses on lateral surface /W	Air heating efficiency
20.16	58.22	4.66	7.55	1.89	81%
16.92	56	5.22	8.55	2.22	78%
15.12	54.89	5.62	9.05	2.34	76%
11.16	51	6.83	10.68	2.45	71%

Table 2

Table2 the temperature comparing between simulation result and test result

Test point	T1	T2	T3	T4	T5	T6	T7	T8	T9	T10	T11	T12	T13	T14	T15
Simulation result / K	326.3	324.1	321.1	296.3	295.1	298.1	297.3	318.2	311.3	318.1	315.3	295.9	316.7	317.6	300.7
Experiment result / K	319.4	318.8	314.0	299.8	296.3	301.2	301.2	314.0	309.3	317.5	315.3	299.7	314.0	307.9	299.3
Error / %	2.1	1.6	2.2	-1.2	-0.4	-1.0	-1.3	1.3	0.6	0.2	0.0	-1.3	0.9	3.1	0.5

Figure(s)

Fig.1

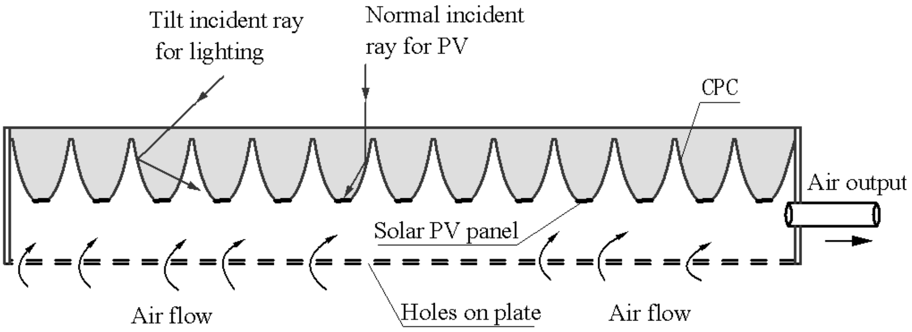

(a) 2D sketch map

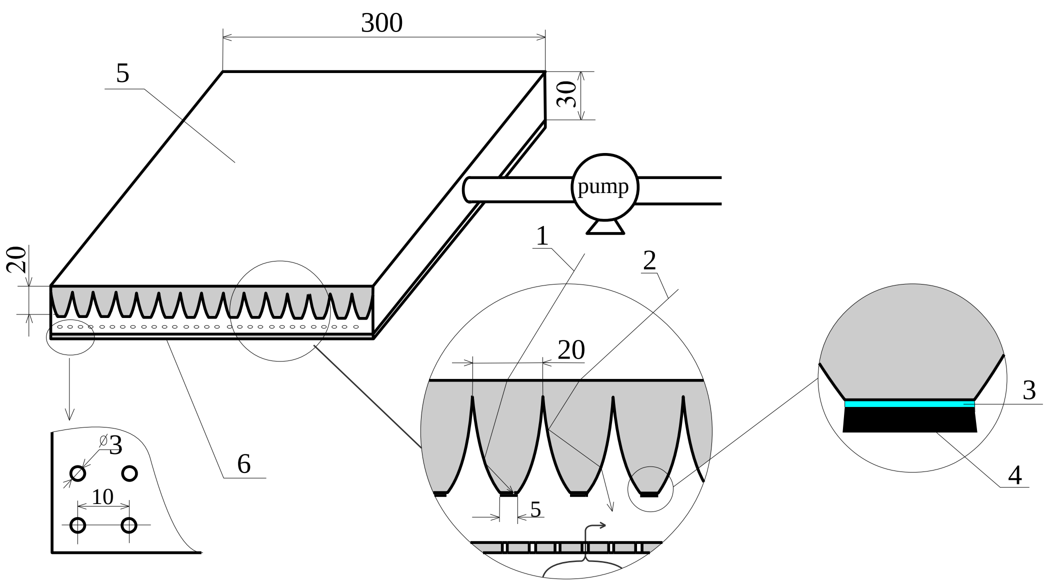

1. Effective generates electricity light; 2.Effective lighting light;

3. Anti-reflection coating; 4.PV cell; 5.Upper cover plate; 6.bottom cover plate

(b) 3D sketch map

Fig.1 The working principle of the PV/T/D device

Fig.2

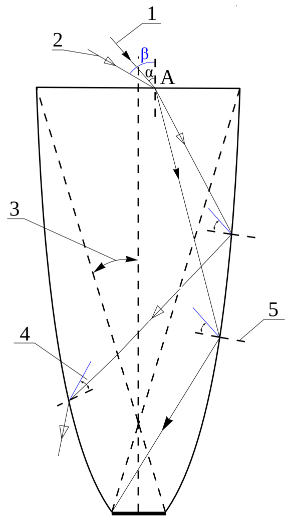

1. Effective generates electricity light; 2.Effective lighting light; 3.Half maximum acceptance angle of entity CPC; 4.Critical angle of total reflection; 5.Surface normal; *A*. Incidence point； *α*,*β*. Incidence angle/°

Fig.2 Entity CPC optical path diagram

Fig.3

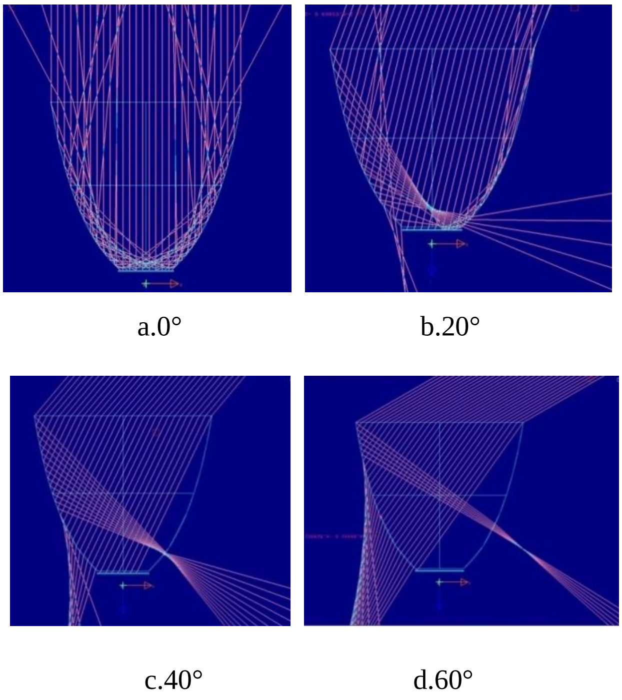

Fig.3 Optical path diagram of different incidence angles

Fig.4

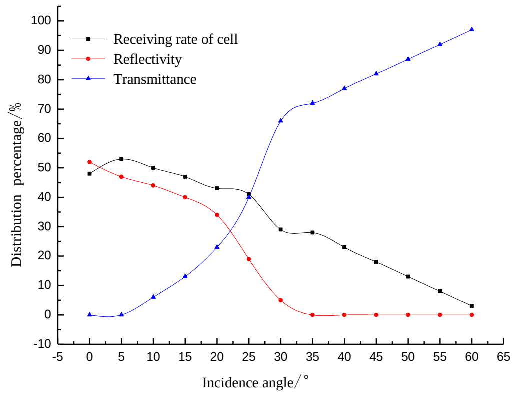

Fig.4 Lights distribution of different incidence angles

Fig.5

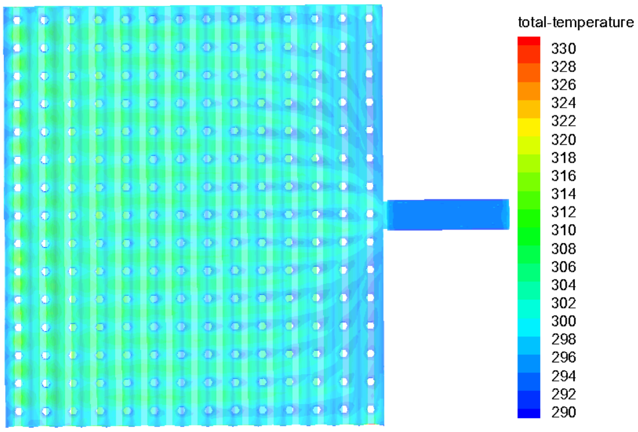

(a) Lower surface

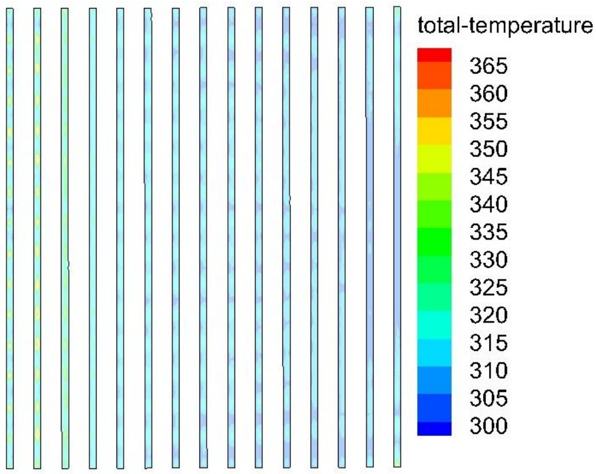

(b) Cell

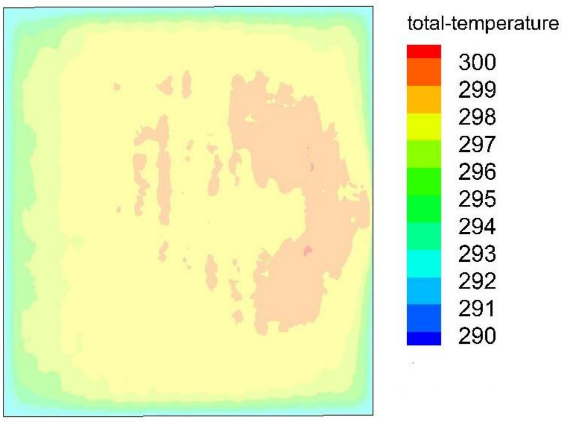

(c) Upper surface

Fig.5 Temperature distribution

Fig.6

Fig.6 the photo of the indoor experimental system

Fig.7

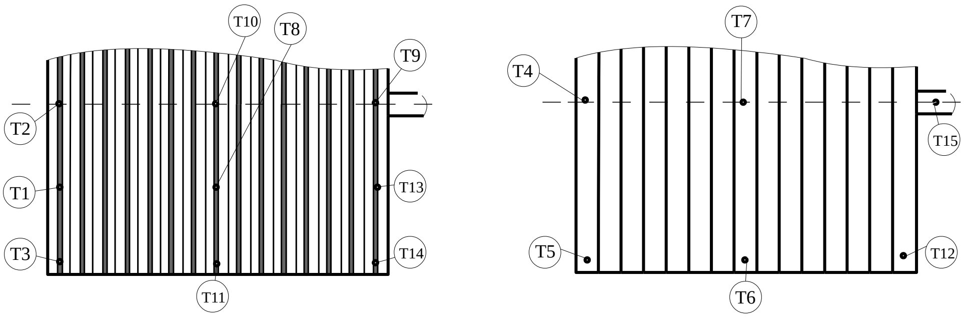

（a）downward view （b）upward view

Fig.7 The arrange diagram of the thermo-couples in the device.

Fig.8

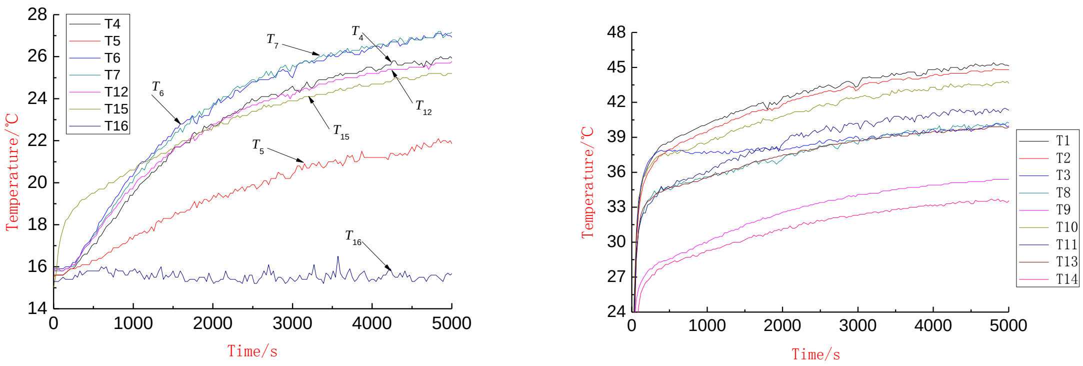

（a）the temperature on up-surface (b) the temperature inside device

Fig. 8 The variation of the temperature in different measuring points with the operation time

Fig.9

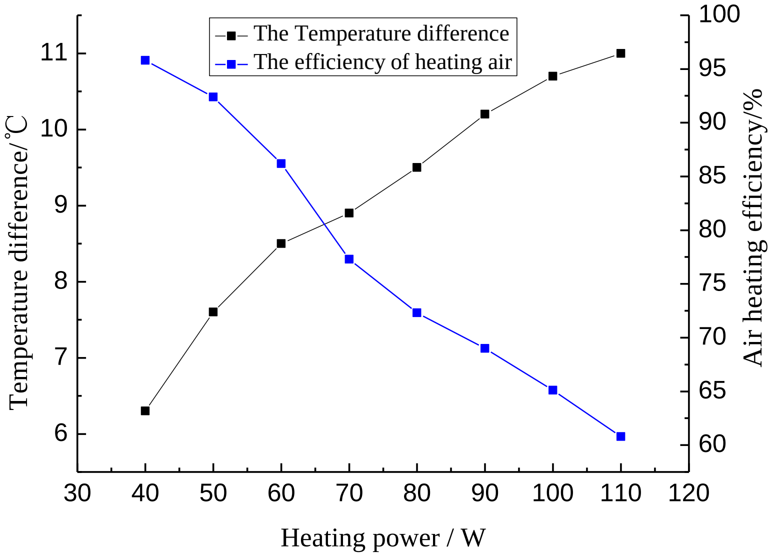

Fig.9 Variation of the Temperature difference between output and input and efficiency under steady state condition with the air heating power

Fig.10

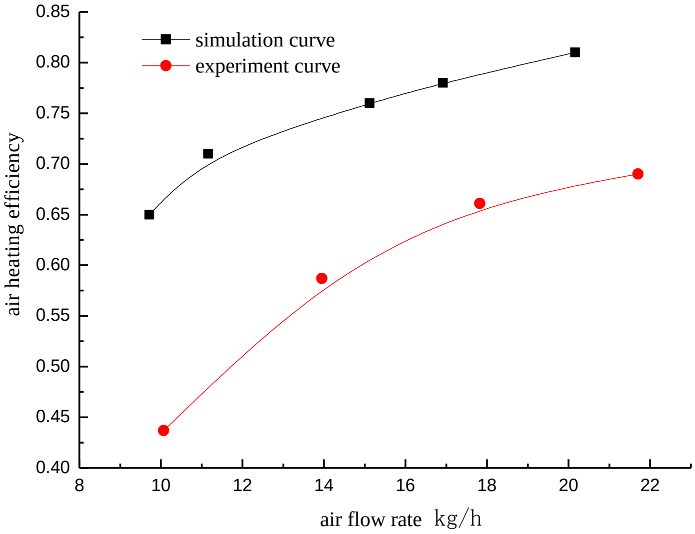

Fig.10 the air heating efficiency comparing between simulation result and experiment result

Fig.11

Fig.11 Experiment system

Fig.12

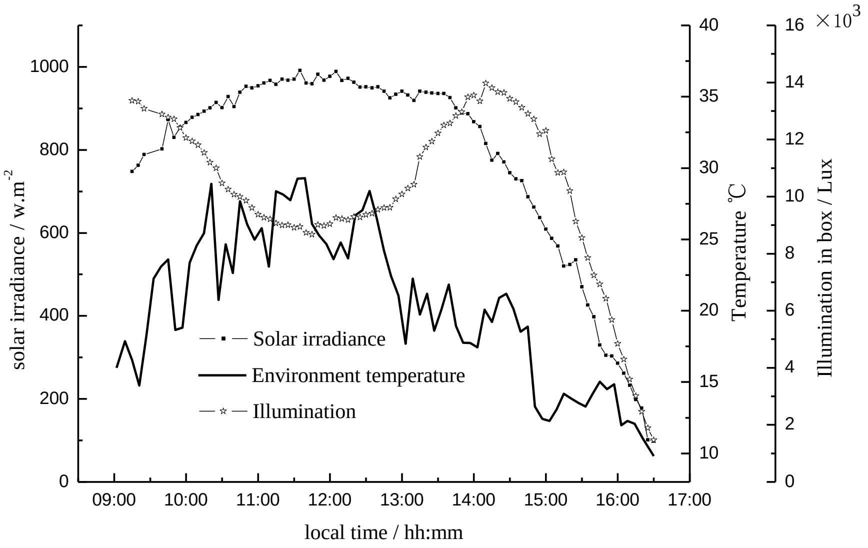

Fig.12 Environment temperature, solar irradiance and integral box illumination

Fig.13

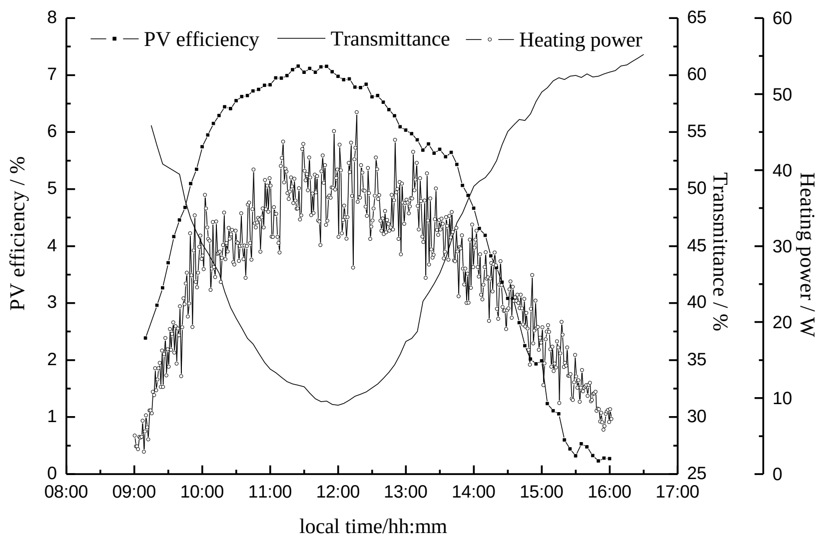

Fig.13 PV efficiency, transmittance and air heating power of the system